1990ApJ...362..674B

THE ASTROPHYSICAL JOURNAL, 362:674–690, 1990 October 20

THE CIRCUMSTELLAR ENVIRONMENT OF THE EMISSION-LINE STAR, LkHα 101[1]

M. BARSONY[2] AND N. Z. SCOVILLE
Owens Valley Radio Observatory, California Institute of Technology
J. M. SCHOMBERT
University of Michigan
AND
M. J. CLAUSSEN
Five College Radio Astronomy Observatory, University of Massachusetts,
and E. O. Hulburt Center for Space Research, Naval Research Laboratory
Received 1989 January 23; accepted 1990 April 17

ABSTRACT

The environs of the pre–main-sequence, emission-line star, LkHα 101, have been observed by broad-band CCD imaging, high-resolution ($\Delta v = 25$ km s^{-1}) optical spectroscopy, *IRAS* imaging, and single-dish, as well as interferometric, millimeter-line mapping.

LkHα 101 exhibits a high mass-loss rate (1.1×10^{-5}) low-velocity (350 km s^{-1}) ionized wind typical of early-type pre–main-sequence stars (Barsony 1989). The millimeter interferometer maps show that this wind has cleared out a cavity in the molecular cloud surrounding LkHα 101, allowing the rapid expansion of the previously observed VLA H II region (Becker and White 1988).

Subject headings: stars: circumstellar shells — stars: emission-line — stars: individual (LkHα 101) — stars: pre–main-sequence — stars: winds

I. INTRODUCTION

It is a well-known, observational fact of millimeter-wave astronomy that molecular cloud line widths are highly supersonic. Among the suggestions for explaining the surprisingly large line widths are cloud collapse, turbulent motions, rotation, or outflowing gas. Claims of large-scale cloud rotation have been shown to be premature upon subsequent closer inspection of the same clouds at higher spatial resolution. Similarly, there is no unequivocal example of a molecular cloud currently collapsing. Recent surveys of small regions of molecular clouds, centered on active, star-forming regions, have led to the discovery of supersonic molecular outflows. LkHα 101 is one of the pre–main-sequence objects searched for signs of a molecular outflow. However, the results for LkHα 101 turned out to be ambiguous, such that no *clear* case for a molecular outflow could be made in this source (Bally and Lada 1983). The unprecedentedly high spatial resolution recently made available with the advent of millimeter-wave interferometry has provided the impetus to examine this source further.

At a distance of 800 pc (Herbig 1971), LkHα 101 is a massive, luminous ($1.2 \times 10^4 L_\odot$; Harvey, Thronson, and Gatley 1979), pre–main-sequence star, a member of the class of "Herbig Be stars." The three defining characteristics of this class are spectral type earlier than A, location in a region of high obscuration, and association with bright nebulosity (Herbig 1960). LkHα 101 lies in a molecular cloud (Knapp *et al.* 1976) and is seen through 9.7 mag of visual extinction (McGregor, Persson, and Cohen 1984). It excites an associated reflection nebula, NGC 1579, and H II region, S222 (Herbig 1956). The directions of the optical polarization vectors in the reflection nebula, NGC 1579, indicate that LkHα 101 is the only significant source of illumination, despite the presence of several nearby embedded T Tauri stars (Redman *et al.* 1986; Becker and White 1988).

The visual extinction in this area is greater than 1 mag over a region almost 1° across and several degrees in declination (Christie, McCutcheon, and Chan 1982). Large-scale CO mapping of this region reveals emission at all observed positions over a 23′ × 24′ area. Molecular line emission over an area coextensive with the visual extinction is inferred (Christie, McCutcheon, and Chan 1982), and *IRAS* data reveal the extent of 100 μm emission in the region to be 33′ east-west by 40′ north-south. H I mapping over a 31′ × 31′ area indicates the presence of $\sim 85\ M_\odot$ of atomic hydrogen with an absorption component near 1 km s^{-1} $V_{\rm LSR}$, which may be due to an H I shell on the near side of the associated dark cloud (Dewdney and Roger 1982). The H I column density distribution can be explained by an equilibrium dissociation model in which H_2 is formed on grains and is dissociated by the UV radiation field of LkHα 101. In order to explain the asymmetry of the H I column density distribution, LkHα 101 must be locally embedded in gas of high density in which there is an opening permitting dissociating photons to escape further on the low-density side. The atomic and molecular gas have not mixed, since the 21 cm line widths are consistently twice as wide as the molecular line widths in the same directions (Dewdney and Roger 1982). Thus, in the H I region, the molecular gas must exist as clumps or cloudlets (see below).

The near-infrared spectrum of LkHα 101 contains bright hydrogen- and helium-emission lines, as well as emission lines of Mg II, Fe II, and [Fe II]. Two distinct emitting regions (both smaller than 3″.75 in size) contribute to the observed spectra (Simon and Cassar 1984): (i) a lower density ($n_e < 10^6$ cm^{-3}), outer circumstellar envelope from which the narrow ($\Delta v = 40$ km s^{-1}) Brackett line and [Fe II] emission originate; and (ii) a high-density ($n_e > 10^6$ cm^{-3}), inner region responsible for the

---

[1] Observations were partially made at the Palomar 60 inch telescope, which is operated by California Institute of Technology and the Carnegie Institution of Washington, and at the Palomar 200 inch telescope, which is operated by California Institute of Technology.

[2] Coinvestigator, *IRAS* Data Analysis Program.

Mg II emission and the broad (>300 km s^{-1}), low-intensity He I and Brγ line components. These authors note that if LkHα 101 were completely surrounded by an ionization-bounded circumstellar envelope, no Lyman continuum photons could escape to ionize the outlying H II region. Based on the radio and hydrogen Brackett and Paschen line emissions of the core component ($<1''$ diameter), the excitation conditions in the ionized gas core are markedly different from those in the surrounding H II region ($\approx 1'$ in extent). To account for the observed ionization of the core by Lyman continuum photoionizations alone would require 100 times greater luminosity in the UV than could be provided by an embedded B0.5 ZAMS star (Harris 1976; Thompson *et al.* 1976). Therefore, other ionization mechanisms, such as ionization by collisions or by Balmer continuum photons, are at work. In fact, the O I line intensities in this source imply that Hα is optically thick (Thompson *et al.* 1976). Thus, the simultaneous presence of a circumstellar envelope that is ionized by collisions or by Balmer continuum photons *and* an H II region that is ionized by the same star is "*prima facie evidence for anisotropic flows near the central star*" (Simon and Cassar 1984).

Herbig (1971) was the first to measure the Hα emission of LkHα 101. A recent spectroscopic study shows that virtually all Herbig Be stars (such as LkHα 101) show Hα in emission, with velocity extents greater than 150 km s^{-1} FWHM (Finkenzeller and Mundt 1984). The Hα emission, in conjunction with detectable radio emission, is interpreted as originating from powerful stellar winds in these stars. Radio continuum observations of LkHα 101 have been made at both high- and low-spatial resolution with the VLA. These data indicate a mass-loss rate in LkHα 101 of 4×10^{-5} $M_\odot$ yr^{-1} in a relatively cool (8000 K), partially ionized, stellar wind (Cohen, Bieging, and Schwartz 1982; Becker and White 1988).

High-velocity wings and line broadening of the ^{12}CO ($J = 1 \rightarrow 0$) line in LkHα 101 were first reported over a decade ago (Knapp *et al.* 1976). Even then, the explanation offered for the line wings was the presence of "random expansion motions about a newly formed H II region" associated with the exciting Be star. In a survey for high-velocity CO line wings carried out with the 7 m Bell Laboratories antenna, LkHα 101 is listed among the "intermediate velocity sources" (10 km s^{-1} $< \Delta v <$ 30 km s^{-1} at $T_A^* = 100$ mK) (Bally and Lada 1983). For these sources, it is unclear whether the observed line widths reflect localized energetic activity, rotation, or turbulent gravitationally bound motion in the ambient molecular cloud. It is the aim of this work to understand the gas dynamics of LkHα 101 in the context of the molecular outflow phase of pre–main-sequence stellar evolution. Observations are described in § II, results are presented in § III, a discussion is given in § IV, and conclusions follow in § V.

II. OBSERVATIONS

a) Optical

i) *Palomar* 1.5 m *CCD Camera and Filter System*

Broad-band images of LkHα 101 and the surrounding region were taken on the Palomar 1.5 m telescope (f/8.8) on 1987 November 16. The transparency was good, with $1\farcs5$ seeing and 20.8 mag arcsec^{-2} sky brightness at 6500 Å. The detector was an RCA CCD with 320×512 pixels. The scale was $0\farcs47$ pixel^{-1}, resulting in a $2\farcm5 \times 4\farcm0$ field. There was no guiding during the exposures, resulting in some minor, but noticeable, elongation of stellar images in each frame.

For various historical reasons, the filter system at the Palomar 1.5 m telescope consists of pseudo-Johnson *B*, Johnson *V*, Gunn *r*, and Gunn *i*, instead of a pure Johnson-Cousins or Kron-Cousins system. This filter set has effective wavelengths of 4200, 5400, 6700, and 8000 Å. The *B* filter is unusual in that it is slightly narrower than a normal Johnson *B* (700 Å FWHM vs. the standard 1000 Å). Consequently, using the Palomar 1.5 m *B* filter results in fewer counts per second, and the color term in the photometric constants is reduced, relative to the standard Johnson *B* filter. This is an awkward setup for any observing program, since two separate sequences of standards must be taken each night to calibrate the blue Johnson filters and the red Gunn filters. It is also difficult to define the Gunn filters properly, since many of the standards from Kent (1985) are too bright ($m < 10$ mag) for the 1.5 m and saturate the chip in the minimum allowed, 1 s exposure time. The standards must, therefore, be taken out of focus, leading to scattered light and overlapping image problems. Another problem for the Gunn system is the very small number of blue standards ($B - V < 0.5$ mag), particularly in the fall sky.

In order to eliminate the problems outlined above, a program was undertaken during the 1986–1987 observing season by one of us (J. M. S.) to transform Landolt (1983) standards onto the Gunn system. A good range of color was selected to develop the zero points and color terms; however, the zero points quoted below are based on the stars HD 19445, HD 140283, and Ross 484 (Bessell 1988). The derived transformations from Cousins to Gunn filters are

$$\begin{aligned} r &= R_c + 0.280 + 0.038(R_c - I_c) , \\ i &= I_c + 0.605 + 0.067(R_c - I_c) . \end{aligned}$$

The reader is cautioned that these transformations are only first-order approximations, sufficient for the data in this study.

The software package ARCHANGEL (Schombert and Wallin 1987) was used for reduction of the raw CCD data. The first step was erase-level subtraction, the erase level being determined from 50 lines of overscan taken after each frame was read out. For exposures longer than 5 minutes, it was also necessary to subtract a dark frame of equal duration to remove noise from a hot amplifier in the upper (north) half of the CCD. These dark frames were collected during the daylight hours and consist of averages of 10 for each exposure time. Flat fields were obtained from dome-illuminated, short exposures taken at least 5 times during the night, and flattening was good to the 0.3% level. Masks were applied to flattened data to flag one bad column and two regions of depressed chip sensitivity. Regions for sky determination were located interactively on a color-graphics display. Normally, these regions would have consisted of several boxes of 20×20 pixels distributed symmetrically around the object of interest. However, LkHα 101 fills most of the CCD frame. From comparison with the Second Palomar Sky Survey IIIa-F plates, a region at the far east end of the absorption lane running south of LkHα 101 was selected for a histogram determination of the sky value in each frame. Judging from the fact that the density level on the Sky Survey plate of this region was identical with density levels well outside the emission nebula, we estimate the photometric error due to sky background to be at the 1% level. This error is negligible for the LkHα 101 data, since most of the nebula has much higher surface brightness. Finally, cosmetic flaws in the chip and cosmic-ray hits were corrected for.

ii) *BVri Photometry*

As mentioned above, the CCD data were calibrated using the standards of Landolt (1983) transformed to the Gunn system. All exposures were 600 s, and were taken with air mass values near 1.0. For stellar objects, the photometry was undertaken using 6″ circular apertures. However, there is a great amount of nebulosity surrounding each star. The choice of 6″ diameter is a compromise between minimizing the amount of light from gas and maximizing the light of the stellar image. Obviously, this constraint serves as the primary source of error for the stellar photometry. Surface photometry measurements for the central nebula were made within a box 1′ on a side, centered on the peak of the extended emission north of LkHα 101. The value for the total luminosity of the nebula is derived from the sum of all the light within the CCD frame minus the contribution of the stellar images. Comparison with new Palomar Sky Survey IIIa-J, IIIa-F, and IV-N plates reveals that only 5% of the total luminosity at optical wavelengths is in the low surface brightness regions outside the CCD field.

iii) *Coudé Spectroscopy*

Two sets of high-resolution optical spectra of the nebulosity associated with LkHα 101 were obtained in the 6550–6750 Å band on the night of 1987 November 15. The observations were made at the coudé focus of the Hale 5 m telescope, with a TI 800 × 800 CCD detector (Gunn, Harris, and Oke 1987). The reflection grating used gave a dispersion of 0.281 Å/15 μm pixel in first order at the 36 inch (0.91 m) focal length "camera" position. Higher orders were filtered out by a 3 mm thick GG495 prefilter. The slit length was 30″ on the sky and was held fixed first in a north-south and next in an east-west position by a dove-prism image rotator. The slit width was 0″.4 on the sky, corresponding to 25 km s^{-1} velocity resolution on the chip. The object was acquired by offsetting from a nearby SAO star. The integration was halted, and the object was reacquired every 15 minutes during the 3 hr integration for the north-south slit position and the 2.5 hr integration for the east-west slit position.

The data were erase-level subtracted, flat-fielded, corrected for atmospheric extinction, and transformed to a flux scale using HD 19445 as the flux standard (Oke and Gunn 1983). The wavelength scale was determined using a Th–Ar comparison arc (courtesy of G. Marcy).

b) IRAS

The *IRAS* survey data were coadded for 25 individual passes over the LkHα 101 region. Fluxes for LkHα 101 in the four *IRAS* bands were determined from the point source filtered FLUX grids (*IPAC User's Guide 1986*). FLUX grid values were corrected for detector nonlinearities, errors that were due to coadd processing, and sampling and position uncertainties. No color correction was applied. The coadd intensity grids were used for determination of the flux from the extended *IRAS* emission, after suitable background level subtraction. An average radial profile of the emission intensity was constructed in each of the four *IRAS* bands by fitting ellipses to the data in logarithmic steps of the radial coordinate.

c) Molecular Lines

i) *FCRAO*

LkHα 101 was observed on 1986 June 9 in the $J = 1 \rightarrow 0$ transition of CO and ^{13}CO with the Five College Radio Astronomy Observatory (FCRAO) 14 m antenna. The HPBW was 45″ at these frequencies. The velocity resolution was 0.27 km s^{-1}. Representative system temperatures were 485 K at ^{13}CO and 753 K at CO. Spectra were obtained by position-switching to $\alpha_{1950} = 04^{\mathrm{h}}29^{\mathrm{m}}30^{\mathrm{s}}$, $\delta_{1950} = 35°30′00″$, a region devoid of emission. The map center coordinates, $\alpha_{1950} = 04^{\mathrm{h}}26^{\mathrm{m}}57^{\mathrm{s}}.23$, $\delta_{1950} = 35°09′54″.9$, coincide with the VLA position of LkHα 101 (Cohen, Bieging, and Schwartz 1982). All offsets marked in the FCRAO maps are in minutes of arc from this reference position. Maps of the molecular emission were obtained on a 9 × 9 element grid, sampled every 15″. Total on-source integration time at each position was 90 s. Data calibration was achieved by inserting an ambient temperature load in the beam.

The SPA (spectral analysis) data reduction program (written by N. Z. S.) was used to produce final maps and spectra of the molecular line emission in LkHα 101. Raw data were corrected for atmospheric and forward-scattering losses ($\eta_{\mathrm{fss}} = 0.72$), with no correction made for the source coupling efficiency since the LkHα 101 molecular cloud is larger than the beam. A constant baseline was fitted to the line-free portions of the spectra, which were subsequently smoothed and rebinned to 1 km s^{-1} resolution.

ii) *OVRO*

Observations of LkHα 101 were made in the $J = 1 \rightarrow 0$ transition of the ^{13}CO molecule with the three element Owens Valley Radio Observatory interferometer during 1985–1986. The synthesized beam was 8″.7 × 6″.3, p.a. −1°.0, and positional errors are estimated to be 20% of the beam size. A flux density of 4.0 Jy was adopted for W3(OH), the amplitude calibrator. The phase calibrator, 2021+317, was observed every 20 minutes. The available filterbank provided 0.136 km s^{-1} velocity resolution, with the central channel tuned to −1.5 km s^{-1} V_{LSR}. Bandpass calibration was achieved using the strong continuum source, 3C 84. Further observational parameters are listed in Table 1. The astronomical image processing system (AIPS) was used to produce the deconvolved source-brightness distributions.

III. RESULTS

a) Optical

i) *BVri Photometry*

The Gunn *i* CCD frame of LkHα 101 is presented in Figure 1. Only three stellar objects appear in all four (*B*, *V*, *r*, and *i*) frames: star A, the northernmost object in Figure 1; star B, in the northeast corner; and LkHα 101 itself. All three have the appearance of being embedded in the neighboring gas and dust. Photometry of the stars marked A, B, and LkHα 101 is presented in Table 2, along with photometric values for the inner nebula (defined by a box 1′ on a side) and the entire nebula. A comparison of the *V* (not shown) and *i* frames is highly suggestive, in that there are 23 more stellar objects in

TABLE 1

OVRO OBSERVATIONAL PARAMETERS

Configuration	Date	LST Range
10E 10W 20N ...	1985 Dec 12	23:16–12:20
20W 00N 30E	1985 Dec 22	23:14–07:09
10W 65W 50W ...	1986 Feb 06	04:20–09:30
10W 65W 50W ...	1986 Feb 11	23:30–05:10
30E 30W 40N ...	1986 Mar 31	00:42–08:07

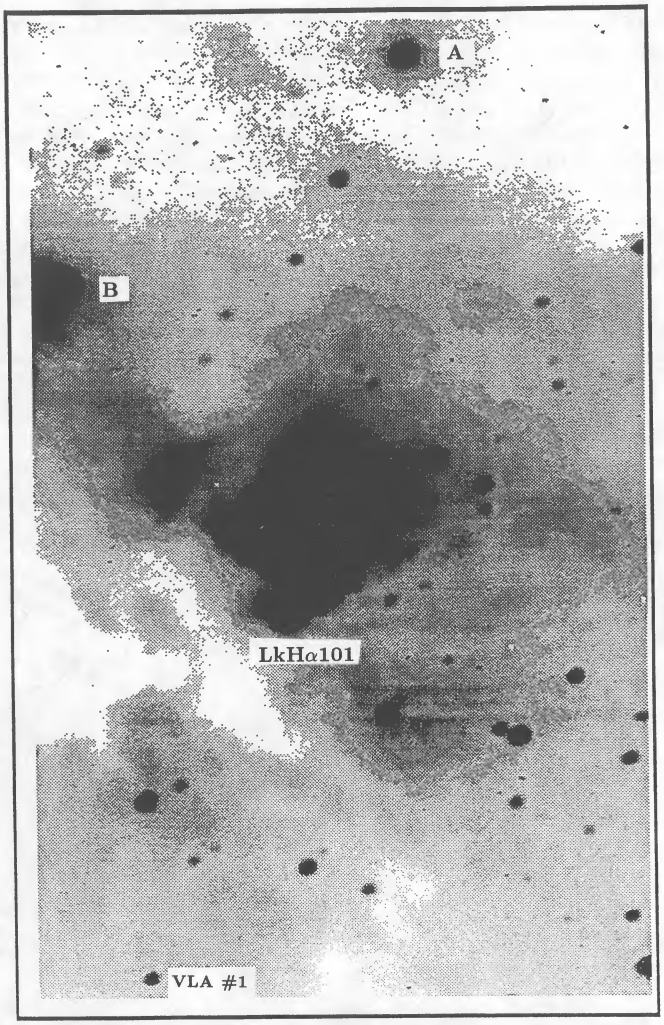

FIG. 1.—Gunn i ($\lambda_0 = 8000$ Å, $\Delta\lambda = 850$ Å) CCD frame of the immediate environs of LkHα 101. At 0.47″ pixel^{-1}, the image scale is 2.′5 × 4.′0. Only the stars marked "A," "B," and "LkHα 101" appear in all the observed bandpasses (B, V, r, and i). Star B is a T Tauri star. The star marked "VLA #1" is a strong candidate for a pre–main-sequence star (see text).

the Gunn i bandpass than in the V. Furthermore, a total of nine weak, compact radio sources in the 8′ × 10′ field centered on LkHα 101 have been reported in a recent VLA study (Becker and White 1988). One of these sources is an extragalactic double. Optical spectroscopy of three of the remaining eight VLA sources shows that two are T Tauri stars and one is a highly obscured B star (Becker and White 1988). Star B of Figure 1 is one of these T Tauri stars. Intriguingly, the star corresponding to Becker and White's VLA source 1 has very red colors. Note that of the three stars, A, B, and LkHα 101, which appear in all four bandpasses, LkHα 101 and star B are both pre–main-sequence objects. Star A has yet to be classified, along with the four remaining compact VLA sources, including VLA source 1. Future spectroscopic work is needed to determine which of these unidentified sources are pre–main-sequence objects.

TABLE 2

OPTICAL PHOTOMETRY

Object	B	$B-V$	$V-r$	$r-i$	D
Star A	16.61	1.43	0.57	0.86	6″
Star B	15.26	1.34	0.48	0.61	6″
LkHα 101	17.66	1.99	1.48	0.91	6″
Central nebula	12.34	0.85	0.57	0.33	1′
Full nebula	10.05	0.73	0.36	0.52	...

ii) *Structure and Color Mapping*

We will present the nebular photometry of LkHα 101 in two ways, cross-sectional analysis and two-color mapping. Figures 2 and 3 display two cross sections centered on LkHα 101, taken north-south and east-west. Each shows a broad range in surface brightness (peaks of 18.3 r mag arcsec^{-2} and troughs of 23.5 r mag arcsec^{-2}). Note the irregular distribution of intensity on small scales. Figure 4 shows the nebular structure after differencing the V and i frames of LkHα 101. For accurate, two-color mapping, a critical step is to register each frame to a common origin to insure that the pixel-by-pixel comparison is not distorted. For the data presented here, there were only three stellar images that appeared through all four filters. These were analyzed for their centroids. Then each set of centers was compared to the B frame set of images, and the corresponding transformations were calculated. Rotation and expansion terms were always negligible, so that only translations were required. The data in each frame were then rebinned into 3″ pixels to increase the signal-to-noise before subtraction. The resulting image for the V and i frames is

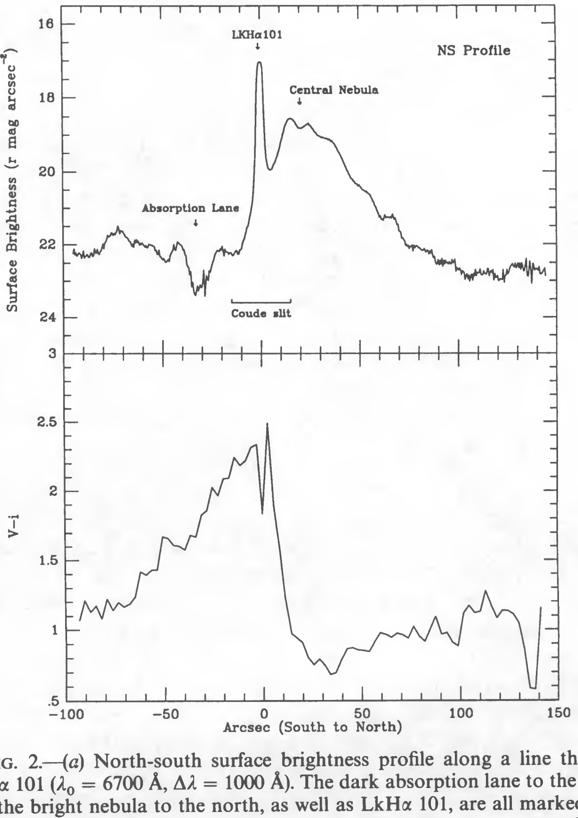

FIG. 2.—(a) North-south surface brightness profile along a line through LkHα 101 ($\lambda_0 = 6700$ Å, $\Delta\lambda = 1000$ Å). The dark absorption lane to the south and the bright nebula to the north, as well as LkHα 101, are all marked. The 30″ long slit, along which the coudé spectra of Figs. 5a and 6 were taken, is indicated. Note the central location of LkHα 101 between the dark lane and the bright nebula. (b) North-south $V-i$ profile along a line passing through LkHα 101. Note the sharp drop right at the position of LkHα 101, indicating its blue color relative to its surroundings. This figure illustrates dramatically how much bluer the bright nebula is, compared with the dark dust lane.

1990ApJ...362..674B

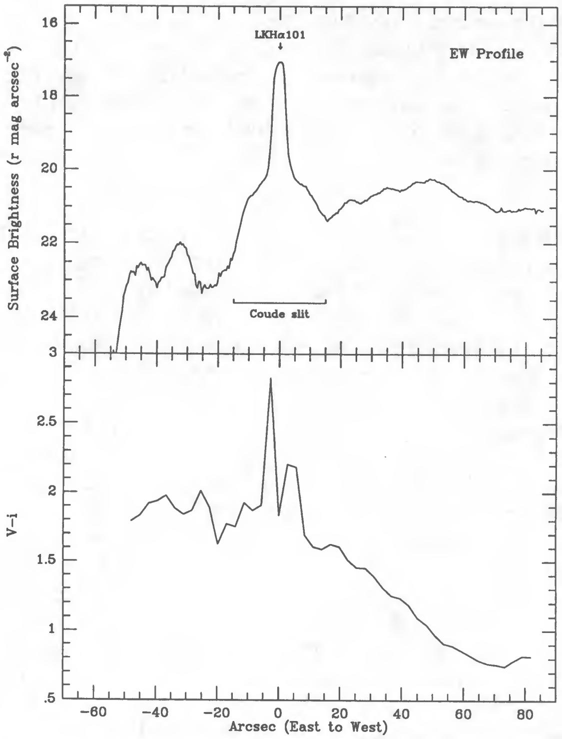

FIG. 3.—(*a*) East-west surface brightness profile along a line through LkHα 101 ($\lambda_0 = 6700$ Å, $\Delta\lambda = 1000$ Å). The position of LkHα 101 is marked, as is the coudé slit position of the spectra of Figs. 5*b* and 7. (*b*) East-west $V - i$ profile along a line passing through LkHα 101. Again, note the sharp drop in $V - i$ color at the position of LkHα 101, confirming its blue color relative to its immediate surroundings, as in Fig. 2*b*.

shown in Figure 4. Visual inspection of this figure reveals a large amount of small-scale structure that is lost in normal intensity maps. In particular, the transition regions from absorption lanes to reflection nebulosity are strongly enhanced. Exact values can be assigned to the gray-scale pixels of Figure 4 by comparison with the cross section colors of Figures 2 and 3. Note that, in general, the dark absorption features are redder than the high surface brightness regions. The high surface brightness regions typically have $V - i$ colors from 0.5 to 1.0, whereas the dark lanes have much redder colors of 2.0 to 2.5. The reddest colors are found around the stars A, B, and LkHα 101.

iii) *Coudé Spectroscopy*

The coudé spectra, integrated over the 30″ slit length, are presented in Figure 5. Because of the presence of high cirrus and the lights of nearby communities, the observed spectral region is riddled with night-sky neon emission lines. These neon lines are marked NS (for night sky) in Figure 5.

Figures 6 and 7 show the coudé slit orientation superposed on the *r* image of LkHα 101 and the variation of the Hα emission profiles with position along the slit. The line profile varies with slit position. The best-fit Gaussian to the Hα profile at the position of LkHα 101 gives a 21 km s^{-1} peak velocity and a 128 km s^{-1} FWHM. This is to be compared with the Brα line at the same position, which has a peak velocity at -2 km s^{-1} and a deconvolved FWHM of 60 km s^{-1} (Persson *et al.* 1984).

We find the Hα line flux to be 26.6×10^{-20} W cm^{-2}. The Brα line flux is 1200 W cm^{-2} (Persson *et al.* 1984). For $T_e = 5000$ K and $n_e = 10^4$ cm^{-3}, the predicted Brα/Hα line ratio is 0.033, assuming the gas is optically thick in the Lyman continuum and that both the Brα and Hα lines are optically thin (Pengelly and Seaton 1964; Brocklehurst 1971; Giles 1977). This implies an extinction of 7.8 mag at Hα, or $A_V = 9.4$ for a $1/\lambda$ extinction law. This determination of the extinction assumes that the $\tau = 1$ surface of the Hα and Brα lines coincide, which is not necessarily the case. Previously derived values for the visual extinction to LkHα 101 are 14.2 (Thompson *et al.* 1977) and 9.7 (McGregor, Persson, and Cohen 1984). Another derivation of the visual extinction is from the molecular hydrogen column density as determined from the FCRAO data. In a 45″ beam, $N_{\rm CO} = 2 \times 10^{18}$ cm^{-2}, which corresponds to $N_{\rm H_2} = 4 \times 10^{22}$, for $N_{\rm H_2}/N_{\rm CO} = 2 \times 10^4$. If we assume all the hydrogen is molecular and that $A_V/E(B-V) = 3.1$, then, using the ratio $N_{\rm H_2}/E(B-V) = 2.9 \times 10^{21}$ molecules cm^{-2} mag^{-1} (Bohlin, Savage, and Drake 1978) leads to a derived *maximum* visual extinction of $A_V = 43$ using this method, since we have assumed *all* the observed gas to be in front of LkHα 101, which is probably not the case.

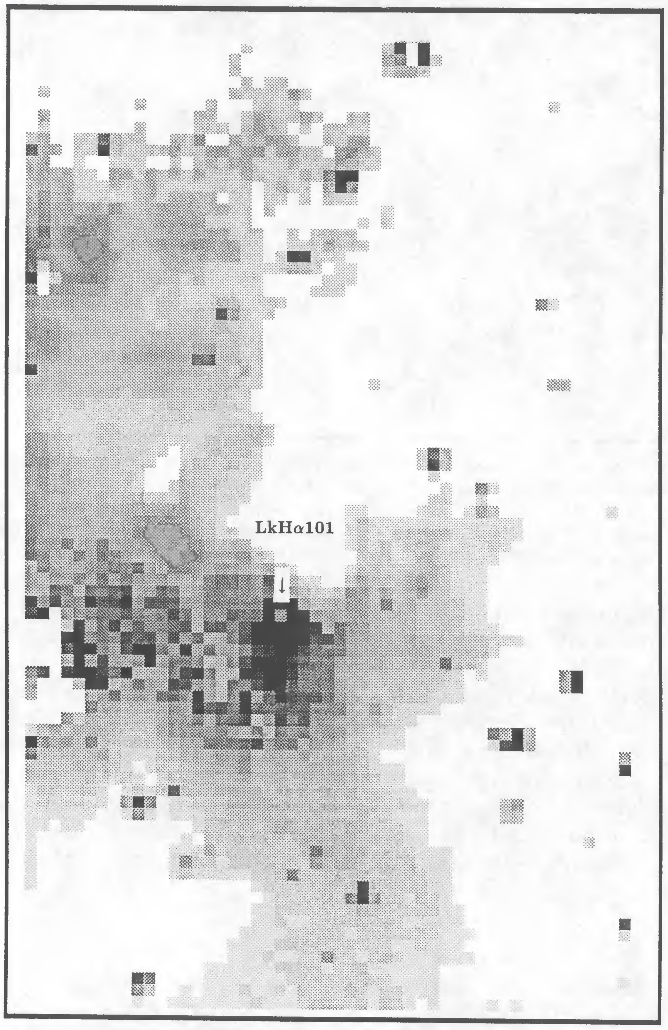

FIG. 4.—$V - i$ map of the LkHα 101 region. North is up; east is to the left. Each pixel is 1″.4 × 1″.4 square. Darker tones indicate redder color. Note the relatively blue color of the pixel containing LkHα 101, standing out from its much redder surroundings. The red dust lane to the southwest appears mottled because of its very low, *V* frame, pixel values. The white (relatively blue) region immediately to the north of LkHα 101 corresponds to the bright nebula.

1990ApJ...362..674B

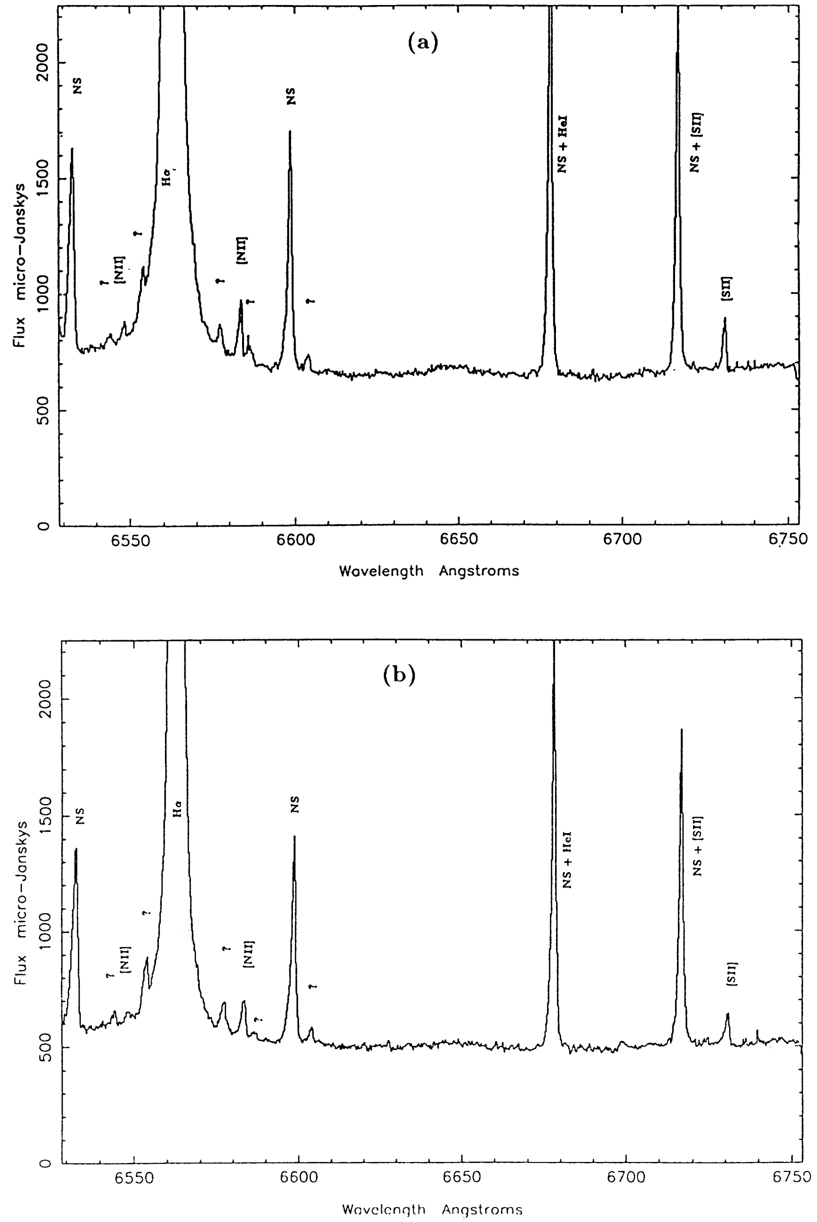

FIG. 5.—(*a*) Coudé spectrum taken through a 30″ long slit running along a north-south direction, centered on LkHα 101. Night-sky neon lines are marked "NS." Question marks indicate the locations of unidentified lines. (*b*) As for (*a*), except that the slit was positioned along a line running east-west.

b) *IRAS*

From the point source filtered coadd survey flux grids (pixel size 1′ × 1′), fluxes in the four *IRAS* bands were 356 Jy at 12 μm, 269 Jy at 25 μm, 2692 Jy at 60 μm, and 3904 Jy at 100 μm. Integration of *all* the extended *IRAS* emission, centered on LkHα 101, from the coadd survey intensity grids, yields fluxes of 1033 Jy at 12 μm, 1228 Jy at 25 μm, 1011 Jy at 60 μm, and 15608 at 100 μm, *including* the contribution of the central "point" source cited above.

The *IRAS* coadd survey intensity maps of the LkHα 101 region are presented in Figure 8. The highest peak intensities in all four bands are located at the position of LkHα 101, showing it to be the dominant source of dust heating in this region. Figure 9 shows the azimuthally averaged radial variation of the *IRAS* emission intensity maps of Figure 8. The straight line above the data points in this figure represents an r^{-3} falloff of intensity with radius. The 100 μm data are best fitted by a constant-density, spherical dust cloud model, with a dust temperature distribution varying as the inverse square root of the radius (Barsony and Najita 1989). However, the 25 μm and 12 μm data cannot be fitted by the same model.

The spectral energy distribution of LkHα 101, from visual to millimeter wavelengths, is plotted in Figure 10. The curve is double-peaked and is empirically well fitted by *three* component blackbodies. All three components are assumed to have dust opacity laws scaling as inverse wavelength for $\lambda < 250$ μm, and as λ^{-2} for $\lambda > 250$ μm. The three input parameters for each blackbody fit are the effective temperature, the 250 μm opacity, and the source size. The best-fit parameters to the optical data are $T_{\rm eff} = 1130$ K, $\tau_{250} = 0.002$, and a source dia-

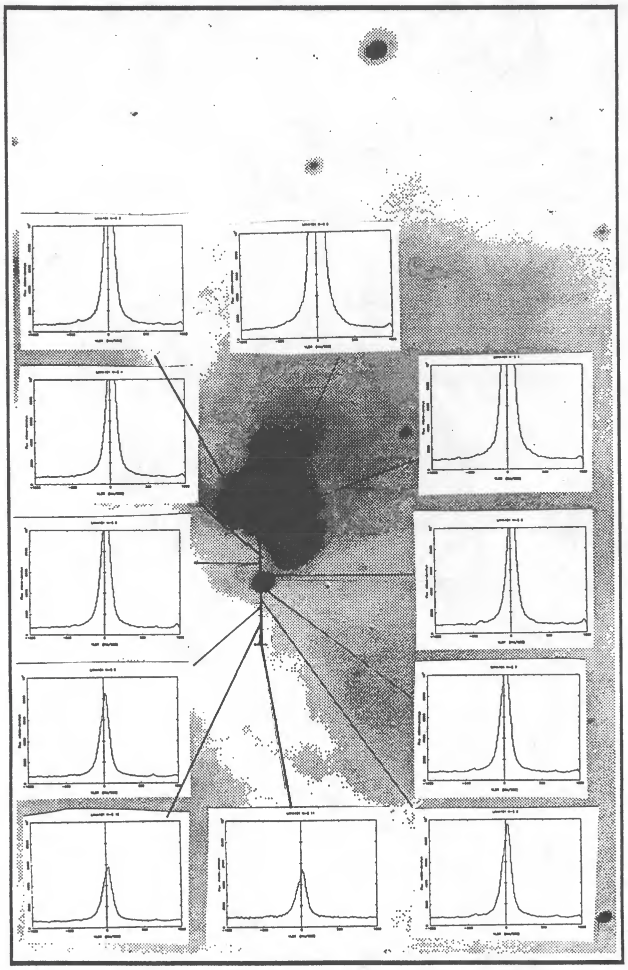

FIG. 6.—Variation of the Hα line profile as a function of slit position along a north-south line centered on LkHα 101 (superposed on *r* image).

meter of 0.″022. The mid-infrared data are fitted with $T_{\rm eff} = 600$ K, $\tau_{250} = 0.2$, and a source diameter of 0.″075. Finally, the *IRAS* data fit a curve with $T_{\rm eff} = 50$ K, $\tau_{250} = 1.0$, and a source diameter of 10″ extent. Such double-peaked spectral energy distributions are seen in other high-luminosity pre–main-sequence stars, which have destroyed their inner circumstellar dust but are surrounded by much larger scale, very cool dust shells (Barsony 1989; Wilking, Lada, and Young 1989).

Integration under the spectral energy distribution of Figure 10 yields a luminosity of 1.09×10^4 $L_\odot$, in good agreement with the previous determination of 1.2×10^4 $L_\odot$ (Harvey, Thronson, and Gatley 1979). The foregoing refers only to the immediate vicinity (within 4000 AU) of LkHα 101. However, as noted in the introduction, infrared emission is detected by *IRAS* over a much larger area in this source (see Fig. 9). The luminosity of the extended *IRAS* emission from LkHα 101 is ∼3 times that of the point source, assuming the shapes of the far-infrared spectral energy distributions to be the same for the extended and the "point source" components. The spatial correlation of the H I and *IRAS* emission is excellent. The H I gas has an emission component with intensity 57 K, FWHM 7.4 km s^{-1}, and central velocity 1.5 km s^{-1} $V_{\rm LSR}$, as well as an absorption component with a peak brightness temperature drop of 43 K, FWHM of 3.4 km s^{-1}, and 1.2 km s^{-1} central velocity. The derived spin temperature for the absorption component is 11 K (Dewdney and Roger 1982). The lowest derived *IRAS* color temperature is 40 K. The molecular gas, if CO is thermalized, is at 15–20 K. The dust is clearly hotter than the gas.

c) *Molecular Lines*

i) *FCRAO*

Contour maps of the integrated CO and ^{13}CO emission are presented in Figure 11. Figure 12 is a map of the column density of CO integrated over all velocities with significant emission superposed on the Gunn *i* CCD frame of the same region. The column densities were derived using equation (A2) of Scoville *et al.* (1986). Note the correspondence between the dust lane and increasing gas column density in the southeast. The derived mass of molecular gas (using eq. [A6] of Scoville *et al.* 1986) in the 2′ × 2′ field centered on LkHα 101 is 112 $M_\odot$.

The line shapes as a function of position are plotted for CO in Figure 13. Although the observed line widths in LkHα 101 are a factor of 10–20 greater than that expected from thermal broadening alone, no low-level, higher velocity wings are seen at the 0.5 K rms level. Our observations confirm the lack of high-velocity wings at the position of LkHα 101 to the 0.1 K level as previously measured with the Bell Laboratories 7 m

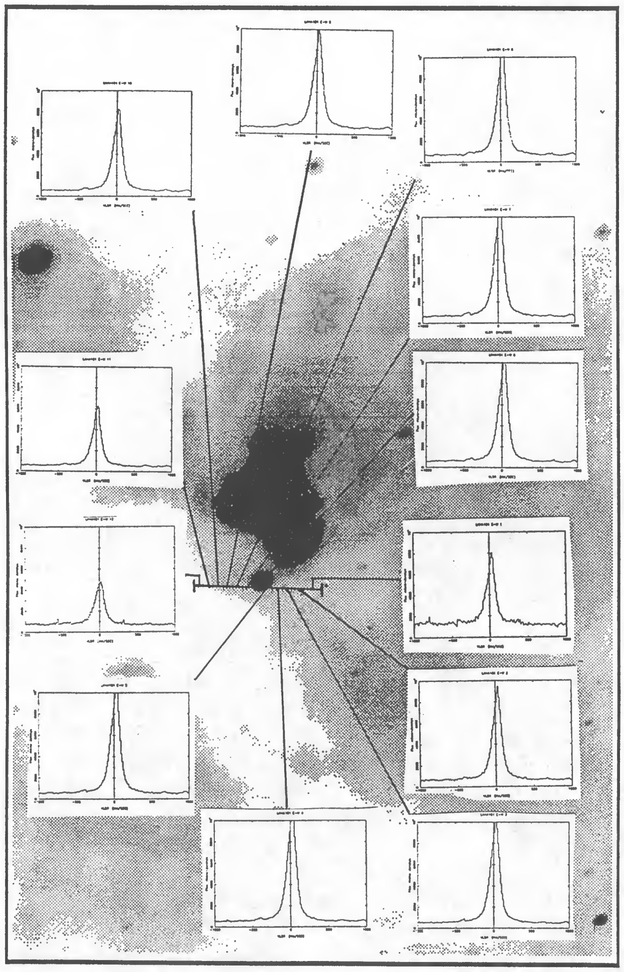

FIG. 7.—Variation of the Hα line profile as a function of position along a slit oriented in an east-west direction and centered on the position of LkHα 101 (superposed on *r* image).

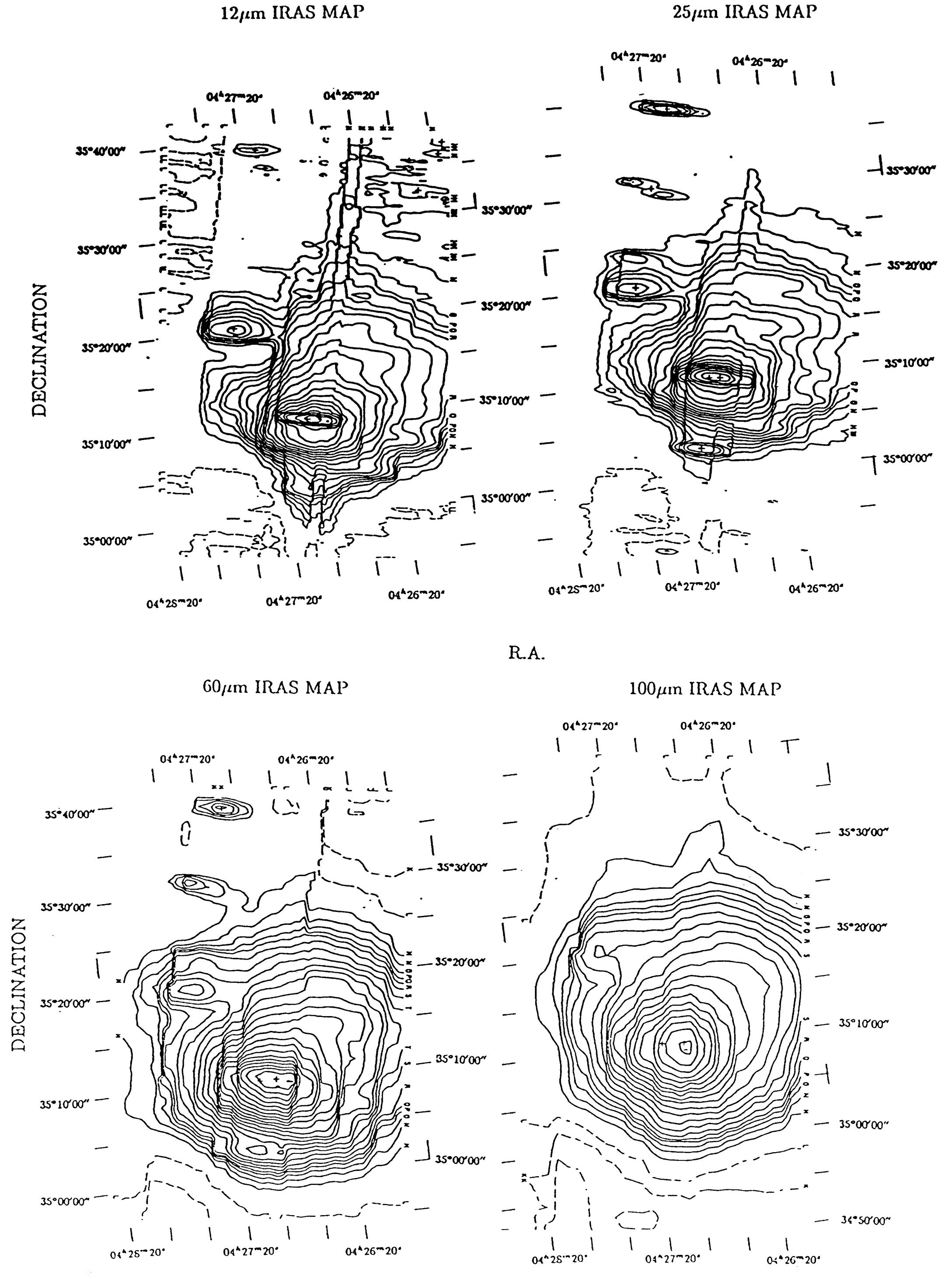

FIG. 8.—*IRAS* survey coadd intensity maps of the LkHα 101 molecular cloud at 12, 25, 60, and 100 μm. Contour level units are W m^{-2} sr^{-1}. Negative contours are indicated by dashed lines and are due to overcorrection by the background level subtraction software. Positive contour levels are at 3.0, 6.0, 9.0, 12.0, 15.0, 20.0, 28.3, 40.0, 56.6, 80.0, 113.1, 160.0, 226.3, 320.0, 452.5, 639.9, 905.0, 1279.8, 1810.0, 2559.6, 3619.9, 5119.2, 7239.6, 10238.2, 14478.8, and 20476.0. Peak contour levels in each of the 12, 25, 60, and 100 μm bands are at 2559.6, 3619.9, 10238.2, and 1810.0 W m^{-2} sr^{-1}, respectively.

telescope (Bally 1982). Thus, there is no evidence in the single-dish data for large-scale, ordered, mass motion, such as would be expected from a molecular outflow source. In particular, there is a definite absence of any *bipolar* outflow. The line profiles in Figure 13 have multiple components. The dip at 0 km s^{-1} V_{LSR} may be due either to two separate clouds along the line of sight or to cool foreground material. The latter case is the more likely one, because of previous evidence for such material from H I data (Dewdney and Roger 1982).

ii) *OVRO*

At the position of LkHα 101, the interferometer detected only continuum emission. The integrated flux from this source is 185 mJy at 2.72 mm. The radio spectrum of the unresolved

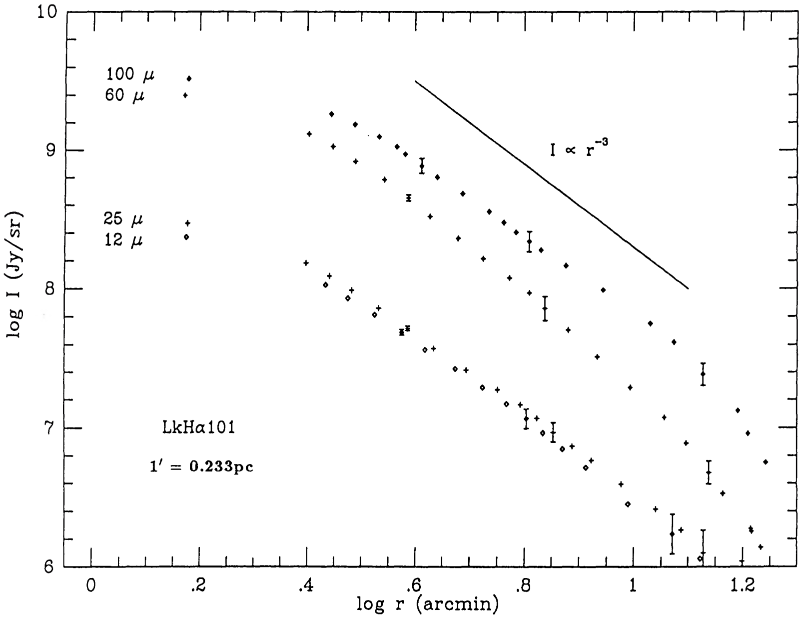

FIG. 9.—*IRAS* radial intensity distribution derived from fitting ellipses to the contours of Fig. 8 in logarithmic steps of the radial coordinate (arcminutes). Note the monotonic decrease in emission strength at all bands with increasing distance from LkHα 101, which shows LkHα 101 to be the dominant heating source in the cloud. Error bars on selected data points are representative for all the data. The intensity profile falling off as r^{-3} is indicated in the upper right-hand corner for comparison with the observations.

core source in LkHα 101 is presented in Figure 14. The best linear fit depicted in this figure has a slope of 0.67 ± 0.05, in good agreement with the $\nu^{0.6}$ dependence predicted for a steady, spherically symmetric stellar wind (Panagia and Felli 1975; Wright and Barlow 1975) and the earlier finding of Cohen, Bieging, and Schwartz (1982).

The ^{13}CO line emission reveals a more complicated source structure (see Fig. 15). We have marked the positions of five "cloudlets" surrounding the continuum source, which coincides with LkHα 101. The total mass in these clumps, for $T_{\rm exc} = 20$ K, is 23 $M_{\odot}$. The spectra of these condensations are

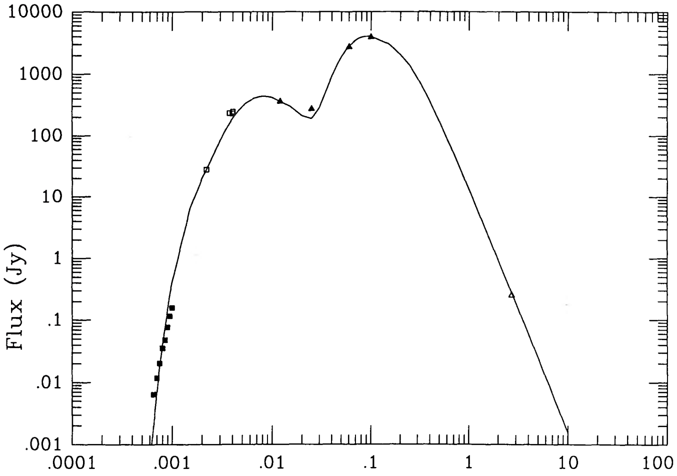

FIG. 10.—Spectral energy distribution of LkHα 101. Filled squares are from McGregor, Persson, and Cohen (1984). The near and mid-infrared data are from Simon and Cassar (1984) and Simon, Simon, and Joyce (1979). Filled triangles are *IRAS* points, and the 2.7 mm flux is from the present work. The solid curve is the best fit to the data and is the superposition of three component blackbodies, as described in the text.

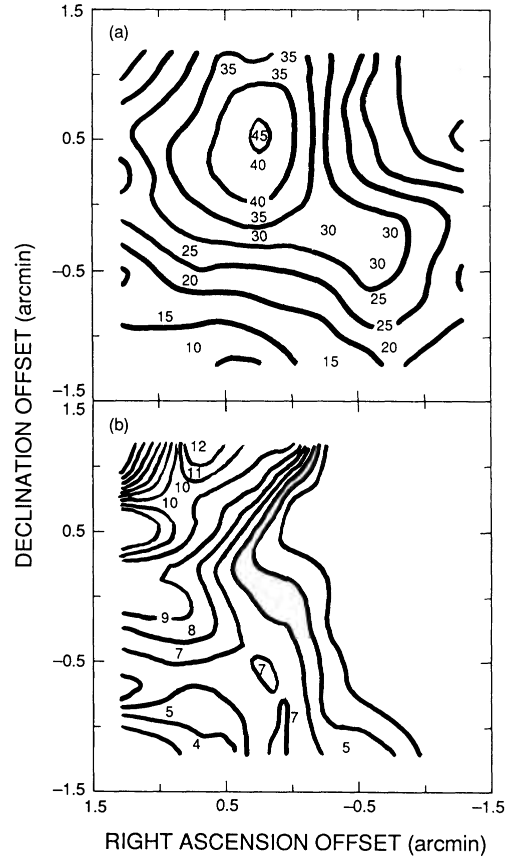

FIG. 11.—(*a*) FCRAO map of the integrated CO emission in a 1′.5 × 1′.5 field centered on LkHα 101 ($\alpha_{1950} = 04^{\rm h}29^{\rm m}30^{\rm s}$, $\delta_{1950} = 35°09′54″.9$). Offsets are marked in minutes of arc from this position. Contour levels are at 10, 15, 20, 25, 30, 35, and 40 K km s^{-1}. (*b*) FCRAO map of the integrated ^{13}CO emission for the same field as in (*a*). Contour levels are at 4, 5, 6, 7, 8, 9, 10, 11, and 12 K km s^{-1}.

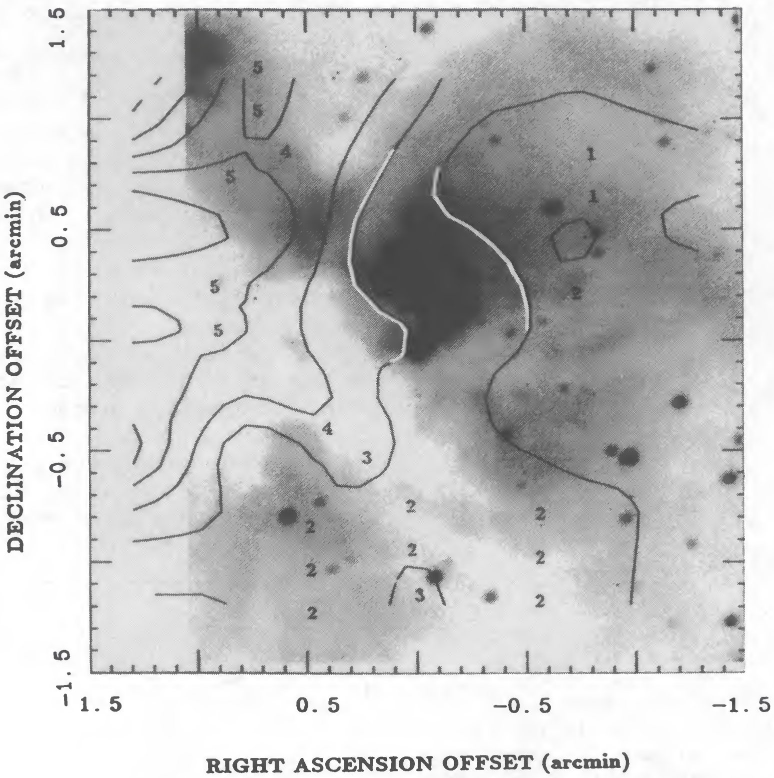

FIG. 12.—Map of the CO column density for the same field as in the previous figure, overlaid on the Gunn *i* image of the region. Contour level units are 10^{18} cm^{-2}. Levels are marked at 1, 2, 3, 4, and 5 times this value. Note the excellent correspondence between the obscuring dust lane and the CO column density contours.

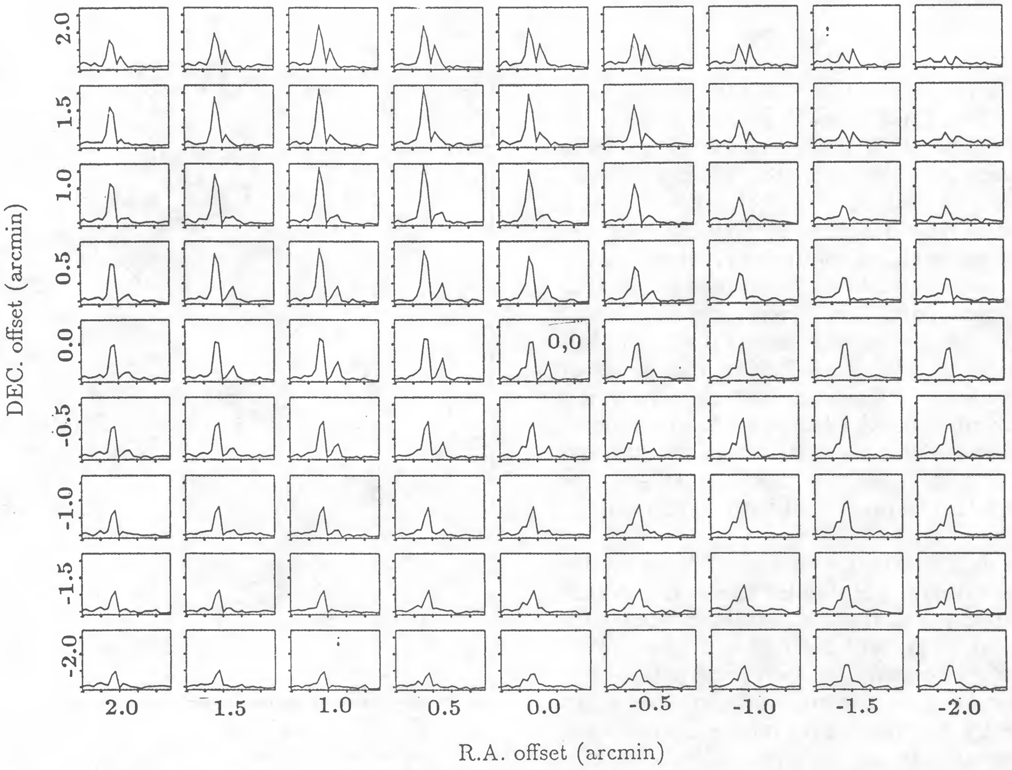

FIG. 13.—Variation of CO line profile with position in the LkHα 101 field as observed with the FCRAO 14 m radio telescope. Vertical axes are in units of T_R^* in 5 K units. Horizontal axes are in units of km s^{-1} $V_{\rm LSR}$, the tick marks indicating 5 km s^{-1} intervals. Note the consistent, self-absorption feature at 0 km s^{-1}, indicating the foreground, cool shell material previously detected in H I 21 cm line observations. From this figure, the marked lack of organized motion, such as would be expected for a bipolar outflow source, is clear.

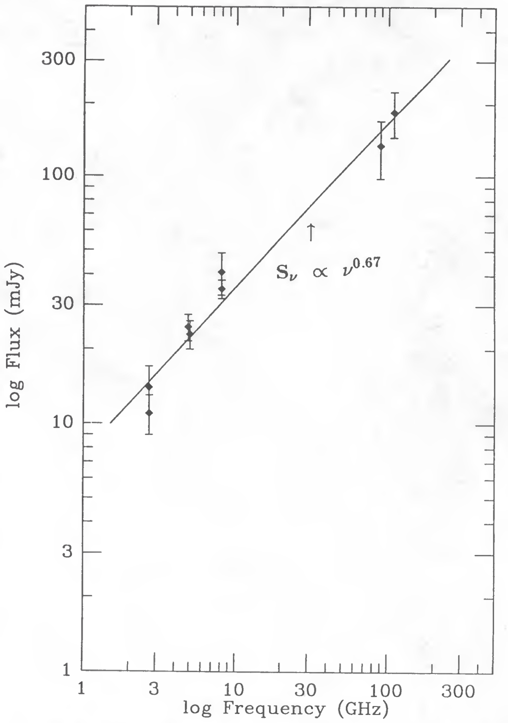

FIG. 14.—Radio spectrum of LkHα 101 from 2.7 to 110 GHz. The 2.7 GHz data points are from Spencer and Schwartz (1974) and Brown, Broderick, and Knapp (1975); the 4.9 GHz data are from Altenhoff *et al.* (1976) and Cohen, Bieging, and Schwartz (1982). The 8.1 GHz points are from Brown, Broderick, and Knapp (1975) and Spencer and Schwartz (1974). The 90 GHz point is from Schwartz and Spencer (1977), and the 110 GHz point is from OVRO (this work). The straight-line fit has a slope of 0.67, indicating $S_\nu \propto \nu^{0.67}$. This slope corresponds to what is predicted for a constant velocity, isotropic, ionized stellar wind.

shown in Figure 16 (solid lines are FCRAO observations, dotted ones are from OVRO). Figure 17 affords direct comparison of the FCRAO and OVRO maps of the region. Here we have direct evidence that the molecular gas distribution near LkHα 101 consists of isolated small "cloudlets," as had previously been inferred from larger scale H I and CO line shapes. Panel 1 of Figure 16 shows that there is general large-scale, blue shifted emission in the line of sight toward cloudlet 1, since the interferometer does not detect emission in the $-3 < V_{\mathrm{LSR}} < 0$ km s^{-1} velocity range, whereas the single-dish observations do. The spectra of panel 2 show the effects of beam smearing of cloudlet 2 in the single-dish data, in which this gas clump is nearly undetected, whereas the interferometer is sensitive to it. Panels 4 and 5 show that both instruments were sensitive to the ridge of molecular emission, which coincides with the dark dust lane so prominent in the Gunn *i* image of Figure 1.

Comparison of the data of Figures 16 and 17 leads to the conclusion that the suprathermal molecular line widths in this region are due to the superposition of many turbulent elements in one single-dish beam. Note that the line widths decrease with the spatial scale of the observation: the interferometer line widths are *always* narrower than the single-dish line widths at the same place on the sky. Turbulent gas motions over at least a factor of 10 in spatial scale are inferred. This turbulent motion is corroborated by the small-scale, sharp variations in the nebular surface brightness apparent in the top panels of Figures 2 and 3.

IV. INTERPRETATION AND DISCUSSION

a) Large-Scale (> 1′) Morphology and Gas Dynamics

i) *Molecular Gas*

It is clear from the foregoing that there is no *molecular* outflow associated with LkHα 101. One might argue that LkHα 101 could have been a molecular outflow source sometime in the past, having already cleared away most of the molecular gas in its immediate vicinity. However, no remnant expansion motions are seen in either the molecular gas or the atomic hydrogen velocity fields surrounding LkHα 101, so any past molecular outflow could have lasted only a very short time. Figure 18 shows the 5 GHz VLA map of LkHα 101 (Becker and White 1988) superposed on the Gunn *i* CCD frame. The dynamical time scale of the extended VLA H II region in the figure is just 1.5×10^4 yr.

A cartoon of the large-scale gas distribution around LkHα 101 is depicted in Figures 19*a* and 19*b* (from Redman *et al.* 1986). The tickmarks in Figure 19*a* indicate arcminute offsets

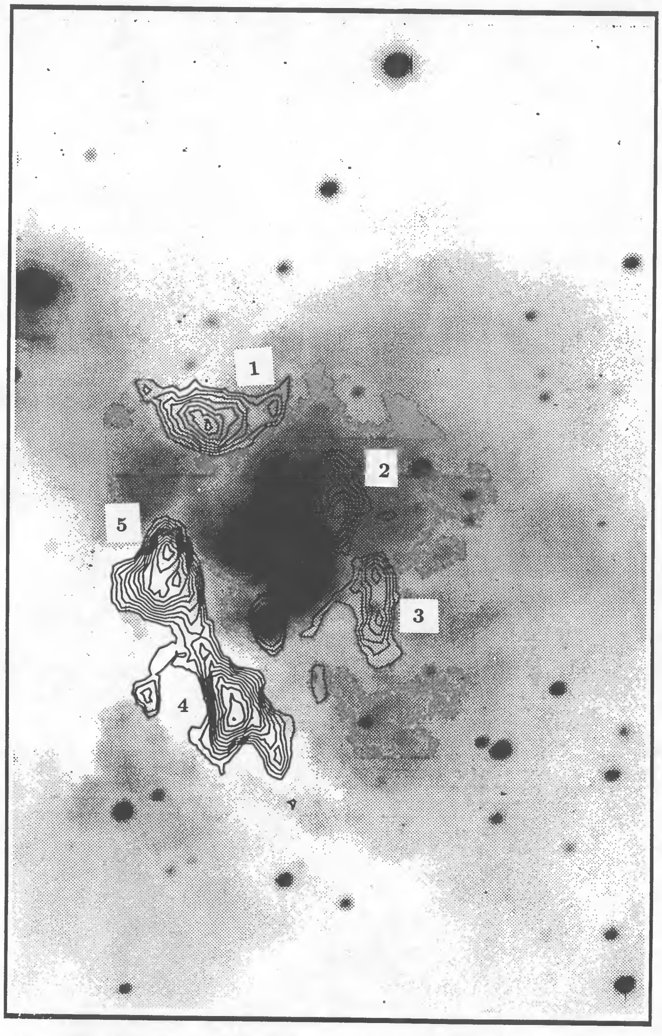

FIG. 15.—Overlay of the ^{13}CO emission detected by the OVRO interferometer overlaid on the Gunn *i* ($\lambda_{\mathrm{eff}} = 8000$ Å) image of the field containing LkHα 101. Note that the central source is *not* line emission, but 110 GHz continuum emission. All the other OVRO contours represent line emission, which breaks up into the "cloudlets" numbered 1–5. Note the clear anticorrelation between the ^{13}CO emission and the brightest part of the nebulosity.

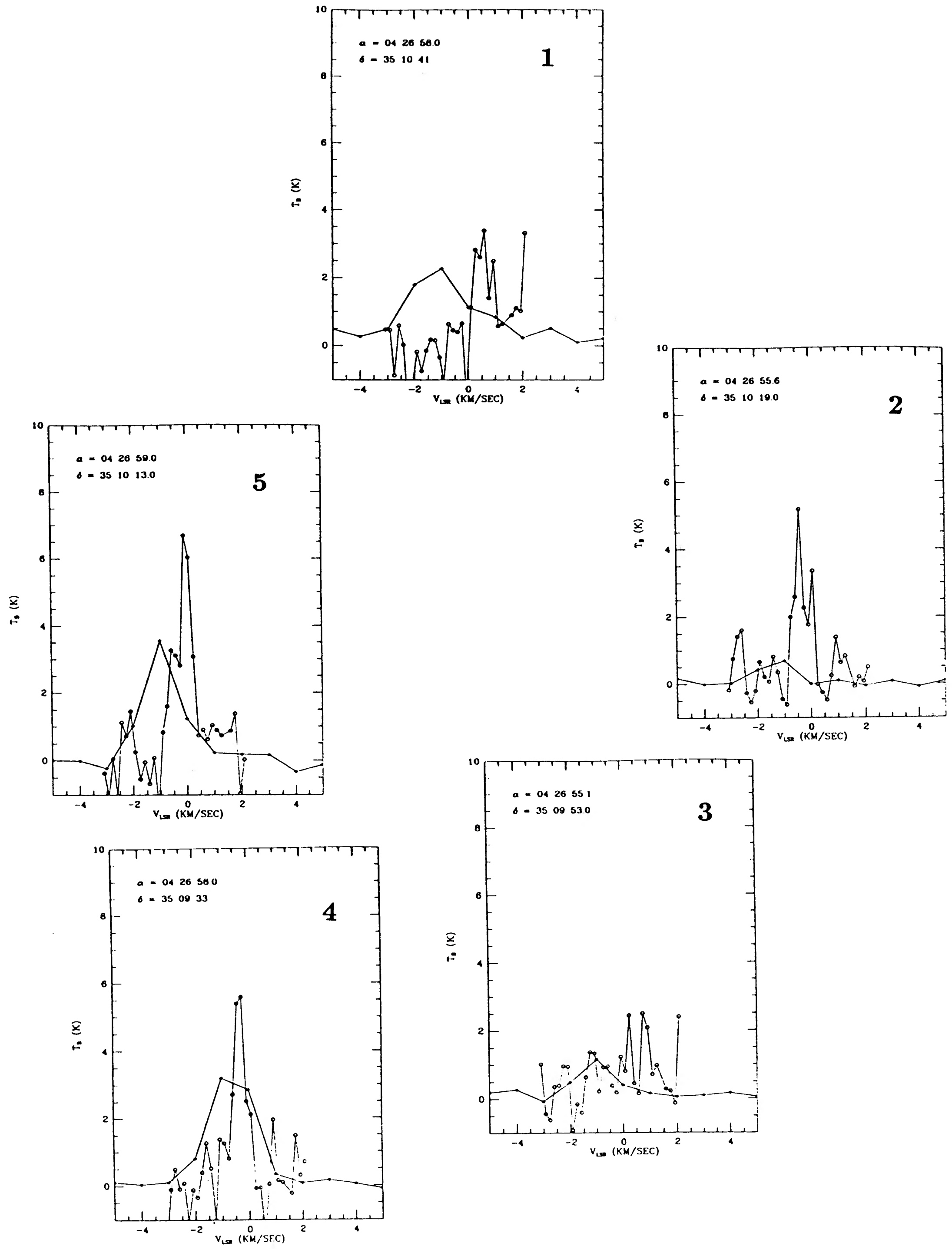

FIG. 16.—FCRAO and OVRO ^{13}CO line profiles of the cloudlets shown in Fig. 15. The numbers in the upper right-hand corners correspond to the numbers assigned these condensations in Fig. 15. The OVRO points may be distinguished by their smaller velocity coverage with respect to the FCRAO data. The position of each spectrum is indicated in the upper left-hand corner of each panel.

from the star. In addition to the sources depicted in this figure, there is a larger scale, cool (10 K) atomic *and* molecular "shell" or cold cloud between us and the LkHα 101 cloud core, which manifests itself as the narrow self-absorption component at about 0 km s^{-1} $V_{\rm LSR}$ in the line profiles of Figure 13, and in H I profiles (Dewdney and Roger 1986). With the higher resolution of the OVRO interferometer observations, the "obscuring cloud," depicted in Figures 19*a* and 19*b*, breaks up into the five cloudlets of Figures 15 and 16. The column density in the "obscuring cloud" is highly variable, ranging from $N_{\rm CO} < 10^{18}$ cm^{-2} to $N_{\rm CO} = 5 \times 10^{18}$ cm^{-2} (see Fig. 12).

ii) *Far-Infrared Emission*

In view of such large-scale inhomogeneities in the gas distribution, it is interesting to note that one cannot characterize the dust and gas by a single kinetic temperature. While the

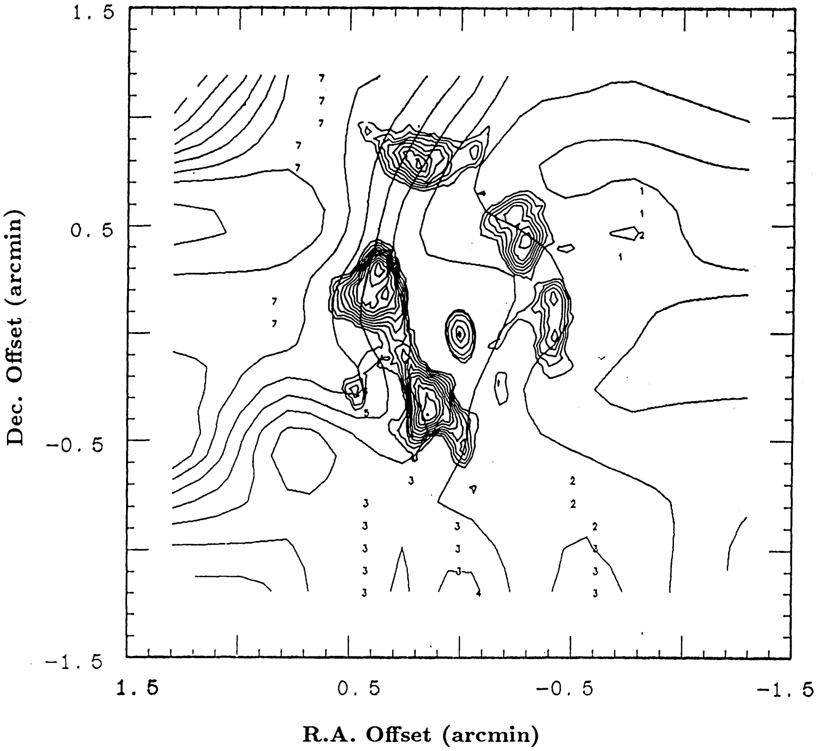

FIG. 17.—Integrated OVRO ^{13}CO emission, with the 110 GHz continuum source at the position of LkHα 101, superposed on the map of integrated ^{13}CO emission as observed with the FCRAO single-dish telescope. When comparing the two maps, note that the OVRO data cover only the central 1′ × 1′ region.

molecular gas is at 10–15 K, a wide range of color temperatures may be inferred from the *IRAS* data of Figure 8. Note, however, that LkHα 101 is *the* chief energy source of the *IRAS* emission in the area, since its position coincides with the positions of the peak emission in all four *IRAS* bands. Using the 100 μm/60 μm flux ratio and assuming a λ^{-1} dust emissivity law, the *IRAS* "point" source color temperature is 42 K, and the extended emission color temperature, excluding this *IRAS* "point" source, is 40 K. Using the 60 μm/25 μm and 25 μm/12 μm flux ratios, derived color temperatures are 58 K and 243 K, respectively, for the "point source," and 61 K and 193 K for the extended emission, excluding the "point source."

We are now left with the problem of explaining the origin of the emission in all four *IRAS* bands. The dust temperature for a grain in equilibrium with a stellar radiation field is given by (Sellgren, Werner, and Dinerstein 1983):

$$T_d = \left(\frac{Q_{\rm UV} L_*}{16\pi\sigma r^2 Q_{\rm IR}}\right)^{1/4} ,$$

where $Q_{\rm UV}$ and $Q_{\rm IR}$ are the Planck-averaged ultraviolet and infrared emissivities, σ is the Stefan-Boltzmann constant, L_* is the stellar luminosity, and r is the distance from the grain to the star. Values of $Q_{\rm UV}/Q_{\rm IR}$ have been determined from observations of the NGC 7023 reflection nebula and are in the range 2000–5000 (Whitcomb *et al.* 1981). Thus, we expect dust temperatures to be between 43 and 53 K 2 pc from LkHα 101, for $L = 4.8 \times 10^4\ L_\odot$ (see below). For comparison, a 30 K blackbody, subtending a circular solid angle of 10′ radius, would emit 2.6 μJy at 12 μm, 310 Jy at 25 μm, 1.63×10^6 Jy at 60 μm, and 8.77×10^6 Jy at 100 μm. The observed integrated fluxes from the emission regions shown in Figure 8 (*including* the central "point" source) are 1033, 1228, 10111, and 15608 Jy at 12, 25, 60, and 100 μm, respectively. The point source fluxes alone are 356, 269, 2692, and 3904 Jy at these wavelengths. Therefore, close to 75% of the emission at each of these wavelengths originates from the extended region. The total luminosity of this extended region is $\sim 3.6 \times 10^4\ L_\odot$. The referee has kindly pointed out that this result is very significant in that it shows that the central object must be of earlier spectral type than B0.V ZAMS, as deduced from the radio data. The *total* luminosity emanating from LkHα 101 is $4.8 \times 10^4\ L_\odot$, the sum of the "point source" and extended emission, which adds up to the luminosity of an O8.5 ZAMS star (Panagia 1973). An O8.5 ZAMS star produces 1.6×10^{48} hydrogen ionizing photons $\rm s^{-1}$ (Panagia 1973), resulting in a 100 AU Strömgren radius if $n_e = 10^7\ \rm cm^{-3}$, or 4.1×10^4 AU for $n_e = 10^3\ \rm cm^{-3}$. The size of the radio continuum envelope observed by the VLA (see Fig. 18) is about equal to the size of this latter Strömgren sphere.

Two questions arise from the *IRAS* data: (1) What is the source of the "excess" 12 μm and 25 μm emission? and (2) How can there be so much cool dust (i.e., 60 μm and 100 μm emission) close in to LkHα 101?

iii) *Optical Emission*

LkHα 101 is viewed through a "hole in the clouds." The large-scale, optical surface brightness distribution in the LkHα 101 region is highly nonuniform and is characterized by high surface brightness filaments, some of which seem to wind azimuthally about the central star. A highly anisotropic distribution of matter near LkHα 101 has been deduced previously. From an analysis of the large-scale, H I column density distribution and the location of its peak, an equilibrium photodissociation model fits the data well "if the star is *locally* embedded in gas of high density with a conical opening towards the northwest" (Dewdney and Roger 1982). This

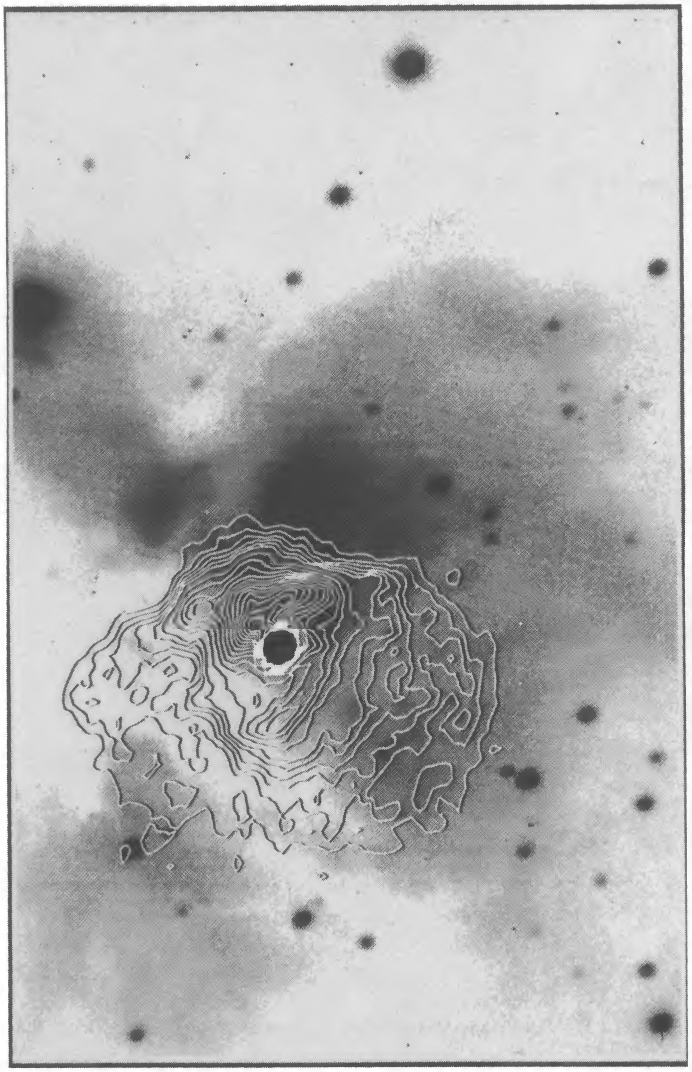

FIG. 18.—VLA 5 GHz map of LkHα 101 overlaid on the Gunn *i* CCD frame (Becker and White 1988). From this figure, we can see that the VLA H II region is behind the intervening obscuring cloud.

result is confirmed by the variation seen in the Hα line profile as a function of slit position in Figures 6 and 7. In both figures, the Hα line profile is much weaker and narrower when viewed through the dust lane to the southeast than when viewed along northwesterly directions.

b) Small-Scale Structure and Gas Dynamics

A simple picture of the small-scale source structure may be deduced from the model fitted to the energy distribution of Figure 10. The three components in this model are an 18 AU diameter, inner region with $\tau_{6500} = 0.8$ and $T = 1130$ K, a 60 AU diameter, intermediate region with $\tau_{6500} = 80$ at $T = 600$ K, and an 8000 AU diameter, outer region with $\tau_{6500} = 400$ at $T = 50$ K. This model is not necessarily physically meaningful. All we have done is to vary the three parameters of temperature, optical depth, and emitting area to match the observed continuum flux in three distinct spectral regions: the optical and near-infrared, the mid-infrared, and the far-infrared and millimeter ranges.

The reddest portion of the nebula ($V - i = 2.2$–2.5 mag) in Figure 4 corresponds to a region of radius ≈6000 AU. LkHα 101 itself forms a blue ($V - i = 1.7$ mag) hole at the center of this red core. This bluer color must be the result of heavy scattering of optical photons near the source. Alternatively, the bluer color at the position of LkHα 101 may be explained by assuming a toroidal or disklike distribution of material surrounding the star, in which case we must be looking at the system nearly pole-on.

A schematic diagram of the "small-scale" structure ($< 1'$) of LkHα 101 is depicted in Figure 20, incorporating all the available observations. Note the surprising variety and number of regions characterized by their different physical conditions. Of special interest is the previously reported "central hole" in the VLA emission (Becker and White 1988), which is coincident within the positional errors of $\pm 1''.1$ in right ascension and $0''.8$ in declination with the relatively blue pixel at the position of LkHα 101 in $V - i$ in Figure 4. The available optical astrometry is not accurate enough to determine whether the peak optical emission from LkHα 101 is offset relative to the best available radio position, however. Any such offset would indi-

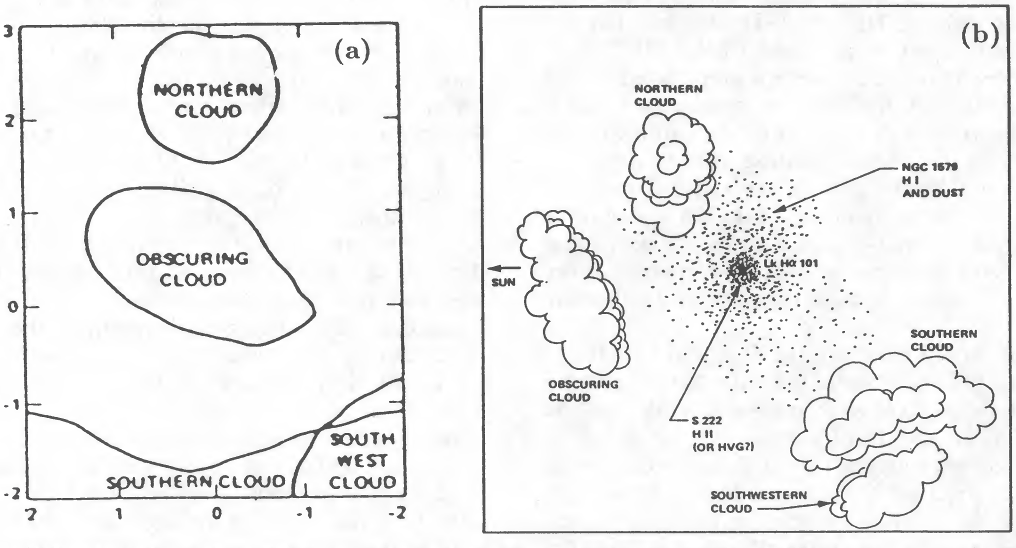

FIG. 19.—(*a*) Schematic representation of the large-scale ($> 1'$) morphology of the gas and dust in the vicinity of LkHα 101 (adapted from Redman *et al.* 1986). (*b*) Side view of (*a*).

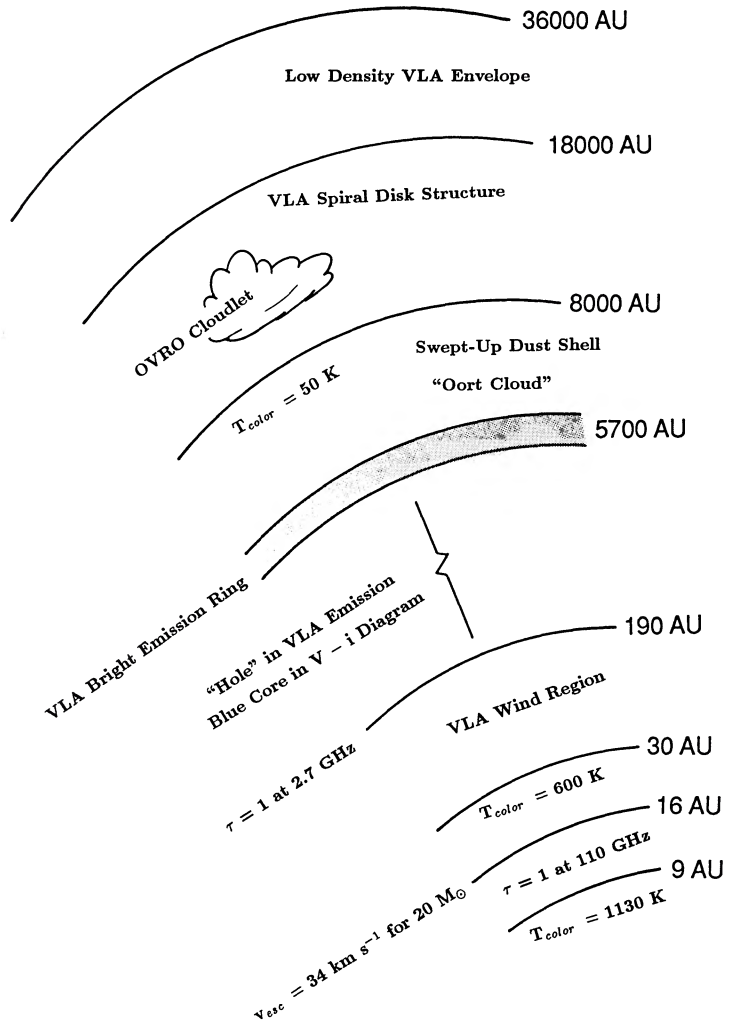

FIG. 20.—Schematic representation of the small-scale structure of LkHα 101 (9–36000 AU), deduced from a combination of infrared, optical, radio continuum, and millimeter-line data.

cate that we are observing scattered, rather than direct, light from the central object.

Based on the similarity of the optical spectra of LkHα 101 and its surrounding nebula, Herbig (1971) argued that the emission-line spectrum must originate at LkHα 101, "while NGC 1579 is no more than a dust curtain illuminated by the star." However, Herbig took the illuminating star to be an F star, whereas we now know it to be closer to O8.5, thus capable of ionizing a large volume of surrounding gas. As noted by Brown, Broderick, and Knapp (1976), the radio continuum appearance of the material surrounding LkHα 101 is part of an emission nebula. Figures 6 and 7 show how highly dependent the Hα line profile is on slit position, which is further evidence for the presence of an emission, rather than a purely reflection, nebula.

At the radio position of LkHα 101, the observed FWHM of the Hα line is a factor of 10 (128 km s^{-1}) greater than the sound speed for a fully ionized, 8000 K H II region, while the line wings extend to ± 350 km s^{-1}, FWZI.

Stellar rotation can be ruled out as the source of the Hα emission-line profile immediately, since rotationally broadened line profiles have a characteristic shape unlike the observed line's sharp peak with extended wings (Rosseland 1936, pp. 202–210). The scattering of Hα line radiation by electrons can also be ruled out as the source of the line wings, since the optical depth for Thomson scattering is 8×10^{-5} for $n_e = 100$ cm^{-3} and a line of sight depth of 8.2×10^4 AU. The optical depth from Thomson scattering in the stellar wind can be estimated by assuming an r^{-2} electron density distribution from the surface of the star out to a diameter of 1200 AU (Cohen, Bieging, and Schwartz 1982). If we take the electron density to have a value of 100 cm^{-3} at 1200 AU and take the inner radius of the wind to be at the stellar surface at 2.1×10^{11} cm, then $\tau \approx 0.1$. Based on this optical depth, Thomson scattering might be a contributing factor to the Hα line width in the central 2″ of the nebula, but it *cannot* account for the large line widths observed throughout the nebula.

Since there is strong evidence from the radio continuum data for the presence of a powerful, ionized stellar wind in LkHα 101, the Hα line wings may be attributed to this wind as well.

Herbig (1971) states that η Car "is the only object known to me whose [optical and near-infrared] spectrum resembles that of LkHα 101, and to a surprising degree of detail. It must mean only that the emitting volumes of the two objects can be plotted at about the same place in the domain specified by n_e,

T_e, and the parameters which describe the radiation field." η Car is an extremely massive ($>100\ M_\odot$) O star, surrounded by a complex of dust, nebulosity, and bright, young, star clusters. As is the case for LkHα 101, the image of the star η Car is decidedly nonstellar and turns out to be a little nebula which is expanding at high speed—about 500 km s^{-1}—from its embedded star. In fact, η Car has passed through several episodes of explosive outbursts (Malin and Murdin 1984, p. 118). By analogy, it is plausible that LkHα 101 is experiencing similar mass-loss episodes, and the Hα line wings are indicative of mass motion in the ionized gas. The observed molecular gas is clearly in the foreground (see Figs. 19*a* and 19*b*) and unaffected by the expanding motions of the ionized gas.

However, discrepancies exist in the line widths and line center velocities of different hydrogen recombination lines. The widths (FWHM) of the Hα, Paγ, Brγ, Brα, and H92α lines are 128 km s^{-1} (this work), 144 km s^{-1} (Ulrich and Wood 1981), 40 km s^{-1} (Simon and Cassar 1984), 60 km s^{-1} (Persson *et al.* 1984), and 17.5 km s^{-1}, respectively, with the Brγ line exhibiting a broad (300 km s^{-1} wide), low-intensity component (Thompson *et al.* 1976; Persson *et al.* 1984; Simon and Cassar 1984; Knapp *et al.* 1976). Simon and Cassar's value for the FWHM of the Brα line is 40 km s^{-1}, in contrast with Persson *et al.*'s value of 60 km s^{-1}. So, again, within the errors, the FWHM values of the Brα and Brγ lines agree and are ~40% narrower than the Hα and Paγ lines. The Brackett line spectra were obtained through 4″ apertures, whereas the Hα and Paγ lines were obtained using slit entrance apertures. The radio recombination line at 8.3 GHz was observed in a 2′.5 beam. These facts taken together indicate a trend of lower velocity with larger radius from the central object.

Systematically varying hydrogen radio recombination line widths have also been observed in the compact H II region, W3(OH). In W3(OH), the observed line widths decrease with increasing frequency, or, equivalently, with decreasing optical depth (Welch and Marr 1987). These authors point out that a consistent explanation of the variation of line width with frequency in that case would require a detailed model of the spatial distribution of dust and electron density within the emission region.

The peak velocities of the hydrogen recombination lines and one helium recombination line in LkHα 101 are +21 km s^{-1} (this work), −30 km s^{-1} (Ulrich and Wood 1981), −1 km s^{-1} (Simon and Cassar 1984), −2 km s^{-1} (Persson *et al.* 1984), and +3 km s^{-1} (Knapp *et al.* 1976) for Hα, He I λ10830, Brγ, Brα, and H92α, respectively. For comparison, the peak velocities of the uncontaminated [S II] line and of the [N II] lines are +22 and +27 km s^{-1}, respectively. The forbidden-line peak velocities are the same as the Hα line peak velocity within the measurement errors of ±5 km s^{-1}.

One possible explanation of the relatively redshifted peak velocity of the Hα line may be differential extinction over the extent of the line. Blueshifted photons are scattered and absorbed more than the light from redshifted gas; thus, we see relatively less emission from the blue side of the line than from the red. Therefore, scattering and absorption have the net effect of shifting the apparent line peak redward. However, this same argument cannot explain the relatively blueshifted centroid value of the 1.08 μm He I line. Clearly, the ionized helium must be located in a different region than the bulk of the Hα emitting gas. The Brackett lines share the velocity of the cloud as a whole, while the radio recombination line, like some of the foreground molecular material, is slightly redshifted relative to the cloud's rest velocity.

V. CONCLUSIONS

A synthesis of new optical, far-infrared, and millimeter-wave data with existing radio maps reveals the circumstellar environment of the massive pre–main-sequence star, LkHα 101 (see Fig. 20). LkHα 101 itself is the source of a powerful, ionized, stellar wind ($\dot{M} = 1.1 \times 10^{-5}\ M_\odot$, $v = 350$ km s^{-1}). The ionized wind in LkHα 101 is surrounded by a swept-up, filamentary dust shell, which simultaneously shields the few remaining molecular gas cloudlets and allows the escape of enough ionizing photons to produce the larger, low-density VLA envelope. The *IRAS* data show that the total luminosity of this object is 4 times greater than previously surmised. In addition to the optical appearance of this source, the far-infrared energy distribution of the associated *IRAS* point source provides further evidence for the presence of an extremely opaque, swept-up dust shell. Beyond this dust shell lies a ring of molecular gas "cloudlets" resolved by the OVRO interferometer. Much of the molecular gas, which must have been present in the immediate vicinity of LkHα 101 during its formation, has by now been ionized and swept away. The remaining molecular clumps, detected by OVRO, must lie along lines of sight protected from the ionizing flux of LkHα 101 by the intervening dust. The OVRO cloudlets overlap regions of low-density ionized gas in projection. Although the entire vicinity of LkHα 101 exhibits extremely red optical colors, the central 3″ × 3″ square pixel at LkHα 101's position is significantly bluer than the surrounding material. This relatively "blue" pixel coincides with a "hole" in the extended VLA emission mapped by Becker and White (1988) and is probably indicative of heavily scattered light. This latter hypothesis can be tested in the future by highly accurate optical and radio astrometry.

M. B. is grateful to D. Backman for help with the *IRAS* data reduction and to J. B. Oke for his patience and perseverance in revealing the secrets of the Hale 5 m coudé spectrograph. Financial support for M. B. from NSF grant AST84-12473 and JPL grant 116-86 is gratefully acknowledged. The Five College Radio Astronomy Observatory is operated with support from the National Science Foundation under grant AST85-12903 and with the permission of the Metropolitan District Commission of the Commonwealth of Massachusetts. We thank Ron Miller of AT & T Bell Laboratories for the SIS junctions used in the OVRO receivers.

REFERENCES

Altenhoff, W. J., Braes, L. L., Olnon, F. M., and Wendker, H. J. 1976, *Astr. Ap.*, **46**, 11.

Bally, J. 1982, in *Regions of Recent Star Formation*, ed. R. S. Roger, and P. E. Dewdney (Dordrecht: Reidel), p. 348.

Bally, J., and Lada, C. 1983, *Ap. J.*, **265**, 824.

Barsony, M. 1989, Ph.D. thesis, California Institute of Technology.

Barsony, M., and Najita, J. 1989, in *Proc. 4th Internat. Workshop of OAC—Napoli, Dusty Objects in the Universe*, ed. E. Bussoletti and A. A. Vittone (Dordrecht: Kluwer), in press.

Becker, R. H., and White, R. L. 1988, *Ap. J.*, **324**, 893.

Bessell, M. S. 1988, private communication.

Bohlin, R. C., Savage, B. D., and Drake, J. F. 1978, *Ap. J.*, **224**, 132.

Brocklehurst, M. 1971, *M.N.R.A.S.*, **153**, 471.
Brown, R. L., Broderick, J. J., and Knapp, G. R. 1975, *M.N.R.A.S.*, **175**, 87P.
Christie, R. A., McCutcheon, W. H., and Chan, C. P. 1982, in *Regions of Recent Star Formation*, ed. R. S. Roger and P. E. Dewdney (Dordrecht: Reidel), p. 343
Cohen, M., Bieging, J. H., and Schwartz, P. R. 1982, *Ap. J.*, **253**, 707.
Dewdney, P. E., and Roger, R. S. 1982, *Ap. J.*, **255**, 564.
———. 1986, *Ap. J.*, **307**, 275.
Finkenzeller, U., and Mundt, R. 1984, *Astr. Ap. Suppl.*, **55**, 109.
Giles, K. 1977, *M.N.R.A.S*, **180**, 57P.
Gunn, J. E., Harris, F., and Oke, J. B. 1987, *Pub. A.S.P.*, **99**, 616.
Harris, S. 1976, *M.N.R.A.S.*, **174**, 601.
Harvey, P. M., Thronson, H. A., and Gatley, I. 1979, *Ap. J.*, **231**, 115.
Herbig, G. H. 1956, *Pub. A.S.P.*, **68**, 353.
———. 1960, *Ap. J. Suppl.*, **4**, 337.
———. 1971, *Ap. J.*, **169**, 537.
Kent, S. M. 1985, *Pub. A.S.P.*, **97**, 165.
Knapp, G. R., Kuiper, T. B. H., Knapp, S. L., and Brown, R. L. 1976, *Ap. J.*, **206**, 443.
Landolt, A. U. 1983, *A.J.*, **88**, 439.
Malin, D., and Murdin, P. 1984, in *Colours of the Stars* (Cambridge: Cambridge University Press).
McGregor, P. J., Persson, S. E., and Cohen, J. G. 1984, *Ap. J.*, **286**, 609.
Oke, J. B., and Gunn, J. E. 1983, *Ap. J.*, **266**, 713.
Panagia, N. 1973, *A.J.*, **78**, 929.
Panagia, N., and Felli, M. 1975, *Astr. Ap.*, **39**, 1.
Pengelly, R. M., and Seaton, M. J. 1964, *Ap. J.*, **127**, 165.
Persson, S. E., Geballe, T. R., McGregor, P. J., Edwards, S., and Lonsdale, C. J. 1984, *Ap. J.*, **286**, 289.
Redman, R. O., Kuiper, T. B. H., Lorre, J. J., and Gunn, J. E. 1986, *Ap. J.*, **303**, 300.
Rosseland, S. 1936, *Theoretical Astrophysics* (Oxford: Clarendon).
Schombert, J. M., and Wallin, J. F. 1987, *A.J.*, **94**, 300.
Scoville, N. Z., Sargent, A. I., Sanders, D. B., Claussen, M. J., Masson, C. R., Lo, K. Y., and Phillips, T. G. 1986, *Ap. J.*, **303**, 416.
Schwartz, P. R., and Spencer, J. H. 1977, *M.N.R.A.S.*, **180**, 297.
Sellgren, K., Werner, M. W., and Dinerstein, H. L. 1983, *Ap. J.* (*Letters*), **271**, L17.
Simon, M., and Cassar, L. 1984, *Ap. J.*, **283**, 179.
Simon, T., Simon, M., and Joyce, R. R. 1979, *Ap. J.*, **230**, 127.
Spencer, J. H., and Schwartz, P. R. 1974, *Ap. J.* (*Letters*), **188**, L105.
Thompson, R. I., Erickson, E. F., Witteborn, F. C., and Strecker, D. W. 1976, *Ap. J.* (*Letters*), **210**, L31.
Thompson, R. I., Strittmatter, P. A., Erickson, E. F., Witteborn, F. C., and Strecker, D. W. 1977, *Ap. J.*, **218**, 170.
Ulrich, R. K., and Wood, B. C. 1981, *Ap. J.*, **244**, 147.
Welch, W. J., and Marr, J. 1987, *Ap. J.* (*Letters*), **317**, L21.
Whitcomb, S. E., Gatley, I., Hildebrand, R. H., Keene, J., Sellgren, K., and Werner, M. W. 1981, *Ap. J.*, **246**, 416.
Wilking, B. A., Lada, C. J., and Young, E. T. 1989, *Ap. J.*, **340**, 823.
Wright, A. E., and Barlow, M. J. 1975, *M.N.R.A.S.*, **170**, 41.

M. Barsony: Department of Astronomy, University of California, Berkeley, CA 94720

M. J. Claussen: Code 4134 C, Naval Research Laboratory, Washington, DC 20375-5000

J. M. Schombert: Department of Astronomy, University of Michigan, Ann Arbor, MI 48109

N. Z. Scoville: Division of Physics, Mathematics, and Astronomy, California Institute of Technology, MS 105-24, Pasadena, CA 91125